A novel square root adaptive unscented Kalman filter combined with variable forgetting factor recursive least square method for accurate state-of-charge estimation of lithium-ion batteries.

ZHANG, M., WANG, S., YANG, X., XU, W., YANG, X. and FERNANDEZ, C.

2022

A Novel Square Root Adaptive Unscented Kalman Filter Combined with Variable Forgetting Factor Recursive Least Square Method for Accurate State-of-charge Estimation of Lithium-Ion Batteries

Mengyun Zhang[1], Shunli Wang[1,*], Xiao Yang[1], Wenhua Xu[1], Xiaoyong Yang[1], Carlos Fernandez[2]

[1] School of Information Engineering, Southwest University of Science and Technology, Mianyang 621010, China;
[2] School of Pharmacy and Life Sciences, Robert Gordon University, Aberdeen AB10-7GJ, UK.
[*]E-mail: 497420789@qq.com

Lithium-ion battery state-of-charge (SOC) serves as an important battery state parameter monitored by the battery management system (BMS), real-time and accurate estimation of the SOC is vital for safe, reasonable, and efficient use of the battery as well as the development of BMS technology. Taking the ternary lithium battery as the research object, based on the second-order RC equivalent circuit model, a variable forgetting factor least square method (VFFRLS) is used for parameter identification and a combination of the square root of covariance and noise statistics estimation techniques to estimate the SOC, to solve the problem of dispersion of the unscented Kalman filter and the error covariance tends to infinity with iterative calculation, thus ensuring the accuracy of SOC estimation. The feasibility and robustness of the algorithm and the battery state estimation strategy are verified under HPPC and BBDST conditions with maximum errors of 1.41% and 1.53%, respectively. The experimental results show that the combined algorithm of VFFRLS and SRAUKF has good robustness and stability, and has high accuracy in the SOC estimation of Li-ion batteries, which provides a reference for the research of lithium-ion batteries.

1. INTRODUCTION

In recent years, environmental pollution and energy sustainability are of increasing concern, and the growth of new energy is already the focus of attention of all countries. [1-3]. Lithium-ion batteries are extensively applied in new energy vehicles, special robots, energy storage, and other fields due to

their high energy density, long cycle life, small size, and rechargeability. [4]. SOC reflects the remaining battery power directly. Improving the estimation accuracy of SOC can effectively prevent the occurrence of safety accidents caused by battery overcharge and over-discharge. [5-7].

Currently, many researchers have studied lithium-ion batteries and proposed many methods for estimating SOC [8-13]. Already existing SOC estimation methods are classified into the below categories: (1) direct measurement method; (2) data-driven estimation method; (3) model-based estimation method [10, 14, 15]. Two common direct measurement methods are the ampere-hour (Ah) integration and the open-circuit voltage (OCV) method [16-19]. The Ah integral method takes the time integral of the current as an indicator of the battery SOC change. In spite of the ease of implementation of this method, since the SOC calculation process is based on an open loop, it leads to the accumulation of measurement errors [20, 21]. Commonly used data-driven methods include artificial neural networks (ANN) and support vector machines (SVM) [22, 23]. The ANN method requires a large amount o f data, the estimation accuracy and convergence speed of SOC depend on the training method and the number of samples. The SVM method provides strong genericization ability and superior prediction accuracy [24, 25], but it is only suitable for single-input and single-output cases. To obtain more accurate SOC estimation, model-based SOC estimation strategies have received much attention [26, 27]. The model-based method mainly includes particle filtering (PF), an extended Kalman filter (EKF), and an unscented Kalman filter (UKF) algorithm [28, 29]. The PF algorithm based on probability distribution theory can handle any nonlinear model and arbitrarily distributed noise. However, it suffers several shortages, such as high computation burden and particle impoverishment [30, 31]. Among the existing studies, the most widely studied model-based SOC estimation method is the EKF algorithm [32, 33]. The EKF algorithm is improved, and the SOC is estimated by the online update of the noise covariance, so an adaptive EKF algorithm is proposed [34, 35]. However, the use of EKF series algorithms inevitably introduces linearization errors, which reduce the battery SOC estimation accuracy. The unscented Kalman filtering, using no-trace transformation to obtain statistics on the covariance of process noise [12, 36], shows fast convergence, highly accurate, and robust SOC estimation compared to EKF. However, a fixed original value of the noise variance cannot be modified to accommodate changes in working conditions, which may lead to inaccurate or even divergent SOC estimation [37-39]. Although the adaptive unscented Kalman filter (AUKF) algorithm has the same accuracy as UKF and solves the problem of increasing estimation error caused by inaccurate model parameters [40-42], the AUKF algorithm cannot determine the semi-positive nature of state covariance and reduce the error caused by noise covariance, resulting in poor accuracy of the final estimation results. Tian et al. proposed a Fractional Unscented Kalman Filtering (FOUKF) algorithm to estimate the SOC estimation performance under different temperature and aging conditions, to test the accurate of the model and the validity of the estimation method. [43]. However, the algorithm is usually limited to the case of Gaussian distribution.

The SRAUKF algorithm is proposed to solve the problems of filter divergence caused by Cholesky's inability to decompose the state error covariance matrix in the standard UKF algorithm, and the problem that the filter error covariance tends to infinity with iterative calculation due to unknown or uncertain noise statistics. Combined with the VFFRLS algorithm, the variable forgetting factor determined by the prediction error is introduced to accurately identify parameters online, which enhances the reliability and accuracy of the results of the estimation. Lastly, the rationality of the proposed

algorithm is verified under hybrid pulse power characterization (HPPC) and Beijing bus dynamic stress test (BBDST) experiments.

2. MATHEMATICAL ANALYSIS

2.1. Second-order RC modeling

Establishing a reasonable and high-fitting battery model is the key to effectively grasping the external characteristics of lithium batteries[26]. In recent years, various battery models have been proposed at home and abroad, such as thermal models, equivalent circuit models and electrochemical models. Among them, the equivalent circuit model is the most widely used. Frequently used equivalent circuit models involve the Rint model, the Thevenin model, the PNGV model, and the second-order RC model. A comparative study of these equivalent circuit models for lithium-ion batteries is given in the literature [44]. Compared with the second-order RC model, the Rint model is not consider the polarization characteristics, so the accuracy of the model is low and can only approximate the ohmic resistance of lithium-ion batteries [45], the Thevenin model is a first-order model, and there are some errors in the dynamic output voltage curve of the model compared with the actual battery output in practice[46, 47], and the PNGV model increases the computation and requires a higher processor for the design, so it is less used in engineering practice[48, 49]. Because of the complex polarization characteristics of the battery, it is proposed that a model with more parallel RC networks in series should have higher accuracy [50].

Through the analysis and comparison of the above three equivalent circuit models, the accuracy, complexity and feasibility of parameter identification are comprehensively considered, this paper selects the second-order RC equivalent circuit model, which has high simulation accuracy, and can accurately simulate the nonlinear characteristics of the battery system. The second-order RC circuit equivalent model can be displayed in Figure 1.
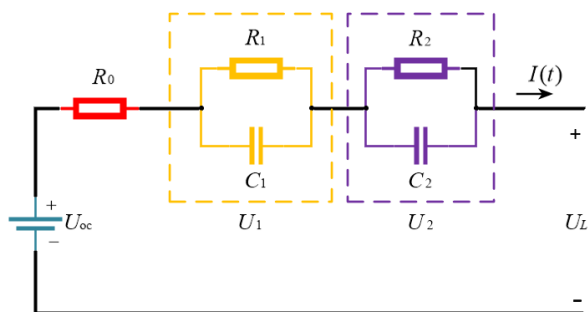

Figure 1. Second-order RC equivalent circuit model

In this model, *Uoc* means open-circuit voltage, R_0 means ohmic resistance, R_1, C_1 means electrochemical polarization resistance and capacitance, and R_2, C_2 means concentration difference

polarization equivalent resistance and capacitance, respectively. $I(t)$ represents the load current, U_L represents the closed-circuit voltage when the battery is connected to a load. By analyzing the circuit structure of the above equivalent model, the knowledge of circuit analysis is applied to obtain its state and observation. From Kirchhoff's voltage law, the mathematical expression of the circuit can be obtained as shown in Equation (1).

$$\begin{cases} U_L = U_{OC} - I(t)R_0 - U_1 - U_2 \\ \dfrac{dU_1}{dt} = -\dfrac{U_1}{C_1 R_1} + \dfrac{I}{C_1} \\ \dfrac{dU_2}{dt} = -\dfrac{U_2}{C_2 R_2} + \dfrac{I}{C_2} \end{cases} \tag{1},$$

where the U_{OC} represents a nonlinear function of the SOC. The definition and discrete expression of SOC can be obtained as shown in Equation (2).

$$\begin{cases} SOC(t) = SOC(t_0) - \dfrac{\eta}{Q_N} \displaystyle\int_{t_0}^{t} I(t)dt \\ SOC_{n+1} = SOC - \dfrac{\eta \Delta t}{Q_n} I_n \end{cases} \tag{2}$$

In Equation (2), $SOC(t)$ represents the current power value at the time t, $SOC(t_0)$ is the initial battery power value, Q_N represents the battery's actual capacity, and η is the Cullen efficiency. Combing Equations (1) and (2), the equation of the state space of the battery SOC is below:

$$\begin{cases} \begin{bmatrix} SOC_{k+1} \\ U_{1,k+1} \\ U_{2,k+1} \end{bmatrix} = \begin{bmatrix} 1 & 0 & 0 \\ 0 & e^{-\frac{\Delta t}{\tau_1}} & 0 \\ 0 & 0 & e^{-\frac{\Delta t}{\tau_2}} \end{bmatrix} \begin{bmatrix} SOC_k \\ U_{1,k} \\ U_{2,k} \end{bmatrix} + \begin{bmatrix} -\dfrac{\eta \Delta t}{Q_N} \\ R_1(1-e^{-\frac{\Delta t}{\tau_1}}) \\ R_2(1-e^{-\frac{\Delta t}{\tau_2}}) \end{bmatrix} \times I(k) + \begin{bmatrix} w(k_1) \\ w(k_2) \\ w(k_3) \end{bmatrix} \\ U_{L,k+1} = U_{OC,k+1} - U_{1,k+1} - U_{2,k+1} - I(k)R_0 + v(k+1) \end{cases} \tag{3}$$

where U_1 and U_2 are the polarized voltages, and U_L is the terminal voltage. Δt is sampling time, τ_1 represents the time constant of the first RC network, which describes the electrochemical polarization process. τ_2 represents the time constant of the second RC network, representing the concentration polarization phenomenon during battery operation, $w(k)$ and $v(k)$ are Gaussian white noises with zero mean value, and selecting $[SOC, U_1, U_2]^T$ as the state variable, U_L as the observational variable.

2.2. Parameter identification based on VFFRLS

Recursive least squares (RLS) is a class of fast algorithms for least squares algorithms, recursive least squares adaptive filters are optimal filters for a set of known data, which can accurately capture the real-time characteristics of the system. It has the characteristics of easy understanding and fast convergence and has been widely used in the field of system identification. Its discrete transfer function and corresponding difference equation are shown in Equation (4).

$$\begin{cases} G(z^{-1}) = \dfrac{y(z^{-1})}{U(z^{-1})} = \dfrac{1 + b_1 z^{-1} + b_2 z^{-2} + \cdots + b_n z^{-n}}{1 + a_1 z^{-1} + a_2 z^{-2} + \cdots + a_n z^{-n}} \\ y(k) = -\displaystyle\sum_{i=1}^{n} a_i y(k-i) + \sum_{i=1}^{n} b_i u(k-i) + v(k) \end{cases} \tag{4}$$

where $U(k)$ and $y(k)$ are the input and output of the system at time point k, respectively. a and b are variables to be evaluated.

The traditional RLS algorithm usually adopts fixed forgetting factor, which does not have sufficient robustness when the algorithm is disturbed. To solve this problem, a novel VFFRLS algorithm is proposed in this study. The forgetting factor in this proposed method is decided by the prediction error and changes adaptably with the handling of the algorithm. The method not only improves the convergence speed of parameter identification when the signal fluctuates or changes sharply but also ensures high identification accuracy when the signal is stable. The calculation procedure of the VFFRLS algorithm is as follows. Equation (5) is the prediction output and estimation error of the model.

$$\begin{cases} \hat{y}(k) = \varphi^T(k)\theta(k) \\ e(k) = y(k) - \hat{y}(k) \\ \theta(k) = \theta(k-1) + K(k)e(k) \\ \varphi^T(k) = \left[-y(k-1), -y(k-2), \ldots, -y(k-n_a), u(k-1), u(k-2), \ldots, u(k-n_b) \right] \end{cases} \tag{5}$$

where $\theta(k)$ represents the parameter vector to be identified, $K(k)$ is the gain, $\varphi^T(k)$ represents a collection of system samples.

The update of the covariance matrix $P(k)$, the forgetting factor $\lambda(k)$ and the Kalman gain $K(k)$ of the battery model after the variable forgetting factor is shown in Equation (6).

$$\begin{cases} P(k) = \dfrac{P(k-1)\left[I - K(k)\varphi^T(k) \right]}{\lambda(k-1)} \\ \lambda(k) = 1 - \dfrac{e^2(k)}{R\left[\varphi^T(k)P(k)\varphi(k) \right]} \\ K(k) = \dfrac{P(k-1)\varphi(k)}{\varphi^T(k)P(k-1)\varphi(k) + \lambda(k-1)} \end{cases} \tag{6}$$

The VFFRLS algorithm for the identification of parameters in the equivalent model of a lithium-ion battery is used to identify the parameters in the second-order RC equivalent circuit model. The battery model is transformed into the mathematical form of least squares as shown in Equation (7).

$$U_{oc} = U_L + \left(\frac{R_1}{R_1 C_1 s + 1} + \frac{R_2}{R_2 C_2 s + 1} + R_0 \right) I \tag{7}$$

Making the time constant $\tau_1 = R_1 C_1$, $\tau_2 = R_2 C_2$, *and* $a = \tau_1 \tau_2$, $b = \tau_1 + \tau_2$, $c = R_1 + R_2 + R_0$, $d = R_1 \tau_2 + R_2 \tau_1 + R_0(\tau_1 + \tau_2)$, $S = [x(k) - x(k-1)]/T$ are substituted into Equation (7) for discretization, whereas sampling time, which is shown in Equation (8).

$$\begin{aligned} U_{oc}(k) - U_L(k) = &\, k_1 \left[U_L(k-1) - U_{oc}(k-1) \right] + k_2 \left[U_L(k-2) - U_{oc}(k-2) \right] + \\ &\, k_3 I(k) + k_4 I(k-1) + k_5 I(k-2) \end{aligned} \tag{8}$$

In Equation (8), $k_1 = \dfrac{-bT - 2a}{T^2 + bT + a}$, $k_2 = \dfrac{a}{T^2 + bT + a}$, $k_3 = \dfrac{cT^2 + dT + aR_0}{T^2 + bT + a}$, $k_4 = \dfrac{-dT - 2aR_0}{T^2 + bT + a}$, $k_5 = \dfrac{aR_0}{T^2 + bT + a}$. Setting $\theta = [k_1, k_2, k_3, k_4, k_5]^T$ as a direct identification parameter, the circuit model parameters R_0, R_1, R_2, C_1, C_2 are then derived from the identification results of these parameters as shown in Equation (9).

$$\begin{cases} R_0 = \dfrac{k_5}{k_2} \\ R_1 = \left(\tau_1 c + \tau_2 R_0 - d \right) / \left(\tau_1 - \tau_2 \right) \\ R_2 = c - R_1 - R_0 \\ C_1 = \tau_1 / R_1 \\ C_2 = \tau_2 / R_2 \end{cases} \tag{9}$$

2.3. Square root adaptive unscented Kalman filtering

When the statistical characteristics of system noise and observation noise change greatly, the SOC estimation accuracy of the UKF algorithm will be greatly reduced. Therefore, the SRAUKF algorithm is proposed, to decompose the covariance matrix in the UKF algorithm by the square root to ensure its non-negative determinism. The process of SOC estimation by SRAUKF is divided into the system prediction and the system update part. The nonlinear system to be disposed of is set up as shown in Equation (10).

$$\begin{cases} x_k = f(x_k, u_k) + w_k \\ z_k = h(x_k, u_k) + v_k \end{cases} \tag{10}$$

In Equation (10), k represents the time, $x_k \in R^n$ represents the state-space variable, and $z_k \in R^n$ reprensents the observation space variable. w_k and v_k reprensent the process noise and measurement noise, respectively. $f(*)$ reprensents a nonlinear function representing the law of state transition, and $h(*)$ reprensents a nonlinear function representing the system state and observation. u_k is the system input at time point k. The calculation procedure of the SRAUKF algorithm is shown below.

Step 1. Initialization. The initialization process is shown in Equation (11).

$$\begin{cases} \hat{x}_0 = E(x_0) \\ P_0 = E\left[(x - \hat{x}_0)(x - \hat{x}_0)^T \right] \\ S_0 = chol(P_0) \end{cases} \tag{11}$$

To determine the state variable and error covariance P_0, and S_0 is the Cholesky factorization of the covariance P_0.

Step 2. The posterior distribution sampling sigma point set based on the k-1 moment is shown in Equation (12).

$$\begin{cases} x_{k-1}^i = \hat{x}_{k-1}, i = 0 \\ x_{k-1}^i = \hat{x}_{k-1} + \sqrt{(n + \lambda)} S_{k-1}^i, i = 1 \sim n \\ x_{k-1}^i = \hat{x}_{k-1} - \sqrt{(n + \lambda)} S_{k-1}^{i-n}, i = n+1 \sim 2n \end{cases} \tag{12}$$

In Equation (12), S_{k-1}^i represents column i of the covariance Cholesky factor at the time k-1 state variable. The corresponding weight values are shown in Equation (13).

$$\begin{cases} W_m^0 = \lambda/(n+\lambda) \\ W_c^0 = \lambda/(n+\lambda)+(1-\alpha^2+\beta) \\ W_i^m = W_c^i = 1/2(n+\lambda) \end{cases} \tag{13}$$

where, $\beta \geq 0$, α is an adjustable parameter that determines the sigma point from the $\hat{x}$ distance, generally takes a smaller integer between 1e-4 to 1, and λ is a scaling parameter, generally defined as $\lambda = \alpha^2(n+\kappa)$-$n$, among $\kappa = 3$-n.

Step 3. Time update. The state variable is predicted by step by the equation of state according to the values of the input variable at time k-1, S_{xk} denotes the updated value of the square root of the error covariance of the state variable at time k as shown in Equation (14).

$$\begin{cases} x_{k|k-1}^i = f\left(x_{k-1|k-1}^i, u_{k-1}\right) + q_k \\ \hat{x}_{k|k-1} = \sum_{i=0}^{2n} \omega_m^i x_{k|k-1}^i \\ P_{x,k/k-1}^- = \sum_{i=0}^{2n} \omega_c^i \left[x_{k|k-1}^i - \hat{x}_{k|k-1} \right]\left[x_{k|k-1}^i - \hat{x}_{k|k-1} \right]^T + Q_k \\ S_{xk}^- = qr\left\{ \left[\sqrt{\omega_c^{1:2n}}\left(x_{k|k-1}^{1:2n} - \hat{x}_{k|k-1}\right), \sqrt{Q_k} \right] \right\} \\ S_{xk} = cholupdate\left\{ S_{xk}^-, \sqrt{abs\left(\omega_c^0\right)}\left(x_{k|k-1}^0 - \hat{x}_{k|k-1}\right), sign\left(\omega_c^0\right) \right\} \end{cases} \tag{14}$$

Step 4. Measuring update. The measurement function output prediction, self-covariance, and mutual covariance are calculated as shown in Equation (15).

$$\begin{cases} y_{k|k-1}^i = h\left(x_{k|k-1}^i, u_k\right) + r_k \\ \hat{y}_{k|k-1} = \sum_{i=0}^{2n} \omega_m^i y_{k|k-1}^i \\ S_{yk}^- = qr\left\{ \left[\sqrt{\omega_c^{1:2n}}\left(y_{k|k-1}^{1:2n} - \hat{x}_{k|k-1}\right), \sqrt{R_k} \right] \right\} \\ S_{yk} = cholupdate\left\{ S_{yk}^-, \sqrt{abs\left(\omega_c^0\right)}\left(y_{k|k-1}^0 - \hat{y}_{k|k-1}\right), sign\left(\omega_c^0\right) \right\} \\ P_{y,k|k-1} = \sum_{i=0}^{2n} \omega_c^i \left[y_{k|k-1}^i - \hat{y}_{k|k-1} \right]\left[y_{k|k-1}^i - \hat{y}_{k|k-1} \right]^T + R_k \\ P_{xy,k} = \sum_{i=0}^{2n} \omega_c^i \left[x_{k|k-1}^i - \hat{x}_{k|k-1} \right]\left[y_{k|k-1}^i - \hat{y}_{k|k-1} \right]^T \end{cases} \tag{15}$$

In Equation (15), S_{yk} is the updated value of the square root of the error covariance at time point k. The filter gain K_k update and the posterior estimation expression are shown in Equation (16).

$$\begin{cases} K_k = P_{xy,k}(S_{yk}, S_{yk}^T)^{-1} \\ \hat{x}_{k|k} = \hat{x}_{k|k-1} + K_k\left(y_k - \hat{y}_{k|k-1}\right) \\ P_{x,k} = P_{x,k|k-1}^- - KP_{y,k|k-1}K_k^T \\ S_k = cholupdate\left(S_{xk}^-, K_k S_{yk}, -1\right) \end{cases} \tag{16}$$

Step 5. The adaptive characteristics of noise statistics as indicated by the Equation (17).

$$\begin{cases} \hat{q}_k = \dfrac{1}{k}\left[(k-1)\hat{q}_k + \hat{x}_k - \sum_{i=0}^{2n} W_i^m f(x_{k-1|k-1}^i, u_{k-1})\right] \\[2ex] \hat{Q}_k = \dfrac{1}{k}\left[(k-1)\hat{Q}_{k-1} + K_k e_k e_k K_k^T + P_{x,k} - \sum_{i=0}^{2n} W_i^c \left[x_{k|k-1}^i - \hat{x}_{k|k-1}\right]\left[x_{k|k-1}^i - \hat{x}_{k|k-1}\right]^T\right] \\[2ex] r_k = \dfrac{1}{k}\left[(k-1)\hat{r}_{k-1} + \hat{y}_k - \sum_{i=0}^{2n} W_i^m (x_{k|k-1}^i, u_k)\right] \\[2ex] \hat{R}_k = \dfrac{1}{k}\left[(k-1)\hat{R}_{k-1} + e_k e_k + P_{x,k} - \sum_{i=0}^{2n} W_i^c \left[y_{k|k-1}^i - \hat{y}_{k|k-1}\right]\left[y_{k|k-1}^i - \hat{y}_{k|k-1}\right]^T\right] \end{cases} \tag{17}$$

In Equation (17), q_k and r_k are the mean matrix of process noise w_k and measurement noise v_k respectively, Q_k and R_k are the variance matrix of process noise and measurement noise respectively. The scheme of SOC estimation by the VFFRLS-SRAUKF algorithm is shown in Figure 2.
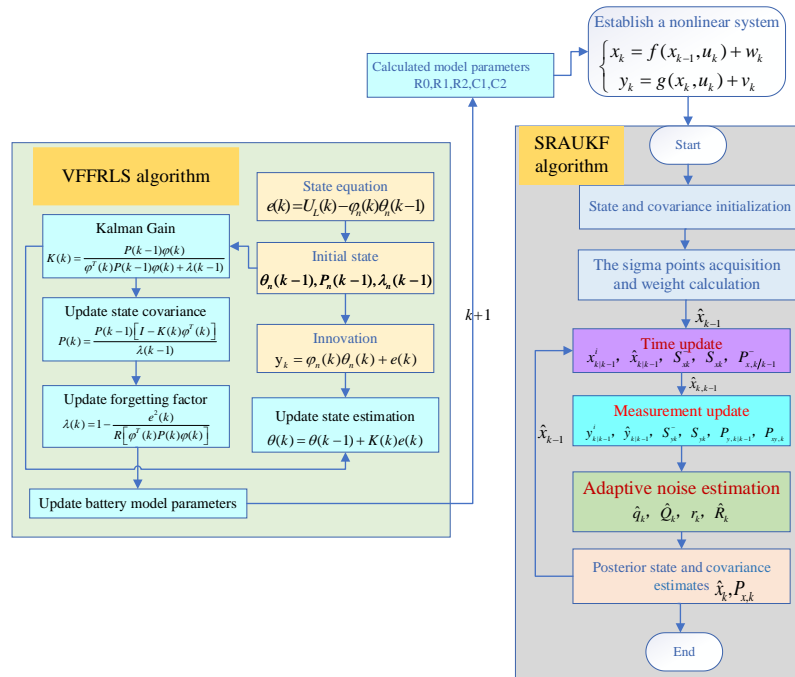

Figure 2. The process of estimation of SOC by the VFFRLS-SRAUKF algorithm

Using the VFFRLS algorithm for parameter identification can effectively improve the accuracy of model parameter identification, and it lays the basis for improving the accuracy of SOC estimation of Lithium batteries.The SRAUKF algorithm uses the square root of the error covariance form update to take the place of the original form of error covariance update, to ensure the symmetry of the error covariance and nonnegative qualitative, in the meantime, using a maximum posterior estimation principle, the output measurement information real-time estimation and correction mean and covariance of the noise, thus ensuring algorithm has the ability of adaptive to change in noise statistical properties. Based on the algorithm, which enhances the tracking effect and stability of the system.

3. EXPERIMENTAL ANALYSIS

3.1. Test platform construction

In this study, a novel ternary lithium-ion battery with a rated capacity of 50Ah is chosen as the experimental target. For obtaining the relevant experimental data, the BTS200-100-104 battery test device and temperature control device provided by Shenzhen Yuyuan Technology Co., Ltd. are used to establish an experimental platform, as shown in Figure 3.
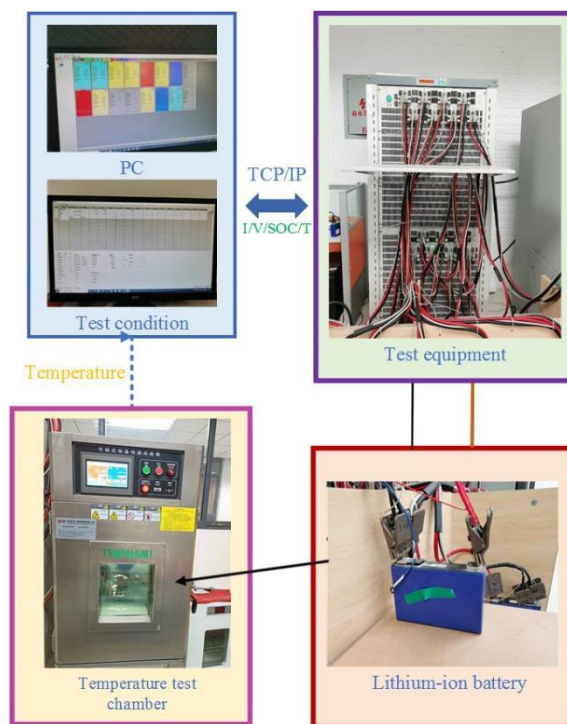

Figure 3. Experimental equipment

3.2. Online parameter identification results

In Refs. [51], a comparative study of multiple models shows that the second-order RC model can exhibit the best performance. Based on the second-order RC model, the test is performed under BBDST conditions using the VFFRLS algorithm. BBDST working condition is an equivalent simulation of the actual working condition of the Beijing bus, mainly including starting, accelerating, coasting, braking, constant speed, rapid acceleration, braking, and so on. The parameter identification results are shown in Figure 4.
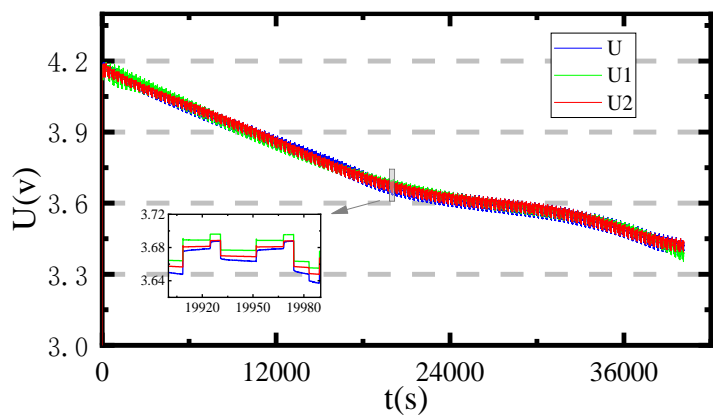
(a) Comparison of parameter identification results of BBDST condition
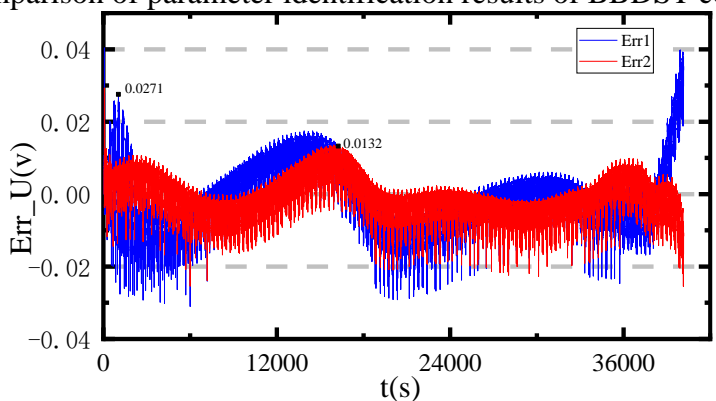
(b) Comparison of parameter identification errors of BBDST condition

Figure 4. Parameter identification results of BBDST condition

Based on the second-order RC equivalent circuit model, reference [52] uses the recursive least square (RLS) method and Kalman filter (KF) on-line identification model parameter algorithm least square method to identify the model parameters, and the estimation error is within the range of [-1.16%, 0.85%]. Reference [53] uses adaptive genetic algorithm (GA) to identify the relevant battery parameters, and the average voltage error is 0.78%, Reference [54] proposed parameter identification with hybrid pulse power characterization (HPPC), which shows that the parameters of 2RC model can be identified in the time domain.

Figure 4 (a) shows the voltage comparison between the RLS and VFFRLS parameter identification results, where U is the actual voltage, U1 represents the analog voltage corresponding to the RLS algorithm, U2 represents the analog voltage corresponding to the VFFRLS algorithm, and it's closer to the actual voltage. Err1 and Err2 in Figure 4(b) respectively represent voltage error curves corresponding to RLS and VFFRLS. It can be seen from Figure 4(b) that the voltage error at the end of charge and discharge in each cycle is large, which is caused by the intense chemical reaction inside the battery during charge and discharge and the lag of voltage following effect. Through algorithm improvement, the fluctuation range of voltage error is significantly reduced, the fluctuation is relatively stable, and the estimation error of VFFRLS is controlled within 0.0132V. Compared with the RLS algorithm, the VFFRLS algorithm can effectively improve the identification accuracy of the model parameters, which lays the grounds for precise estimation of the SOC of the lithium battery.

3.3. Complex condition experiment

To confirm the operating effectiveness of the proposed algorithm on lithium-ion battery SOC estimation under complex application conditions, the HPPC working condition is selected to verify the algorithm. In the actual application process, the lithium-ion battery is mostly worked in the intermittent cycle charge and discharge state. HPPC working condition includes long charging, discharge, and shelving, which can better simulate the actual operation condition of the battery. the estimation results and errors for the different algorithms are shown in Fig. 5.
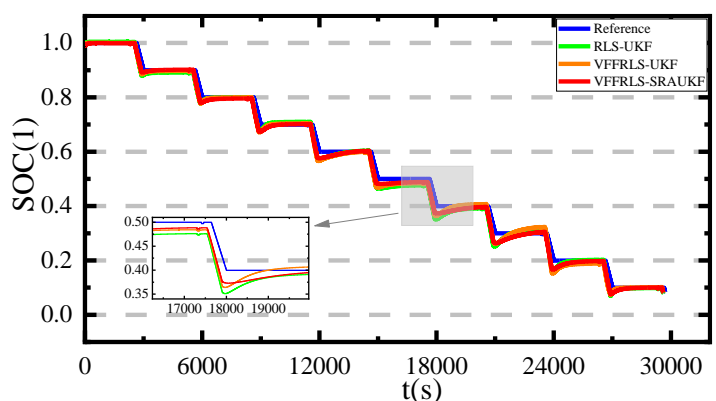
(a) Estimation results of SOC under HPPC condition with different algorithms
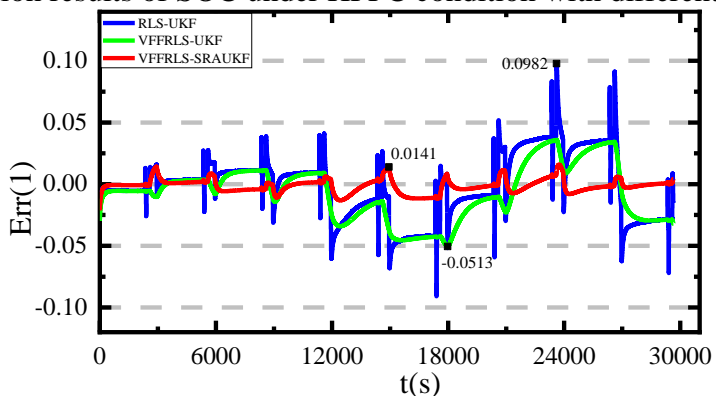
(b) Estimation errors of SOC under HPPC condition with different algorithms

Figure 5. Estimation results of SOC under HPPC operating condition

Fig. 5 (b) shows the error in estimating SOC with three algorithms. With a poor convergence, the maximum error of the RLS-UKF algorithm is about 9.82%. The maximum error of the VFFRLS-UKF algorithm is 0.0513%, and the estimation accuracy is higher than that of RLS-UKF, but the stability is not high. The VFFRLS-SRAUKF algorithm has the best performance, with a maximum error of about 1.41%, which greatly improves the accuracy of the SOC estimation. Combined with Fig. 5 (a) and (b), the VFFRLS-SRAUKF algorithm brings the estimated results closer to the reference value, the algorithm has good convergence, can track the actual value well, and attain favorable estimation accuracy. The maximum (MAX) error, mean absolute error (MAE), and root means square error (RMSE) comparisons of SOC estimation using the three algorithms are shown in Table 1.

Table 1. Comparison of SOC estimation results of different algorithms under HPPC conditions

Estimation method	RLS-UKF	VFFRLS-UKF	VFFRLS-SRAUKF
MAX error	9.82%	5.13%	1.41%
MAE	2.06%	1.89%	0.42%
RMSE	2.58%	2.33%	0.55%

It is displayed in Table 1, the MAE of the VFFRLS-SRAUK algorithm is 0.42%, and the MAE of VFFRLS-UKF and RLS-UKF is 1.89% and 2.06%, respectively, indicating that the VFFRLS-SRAUKF algorithm has minimal estimation error and good identification accuracy. The value of RMSE for the VFFRLS-SRAUKF algorithm is 0.55%, and it is much smaller than the remaining two algorithms, namely, the error volatility range is much smaller than the remaining two algorithms. Overall, the algorithm has high-level stability and non-divergence in the SOC estimation procedure, which proves that the VFFRLS-SRAUKF algorithm can effectively maintain the stability of the estimation.
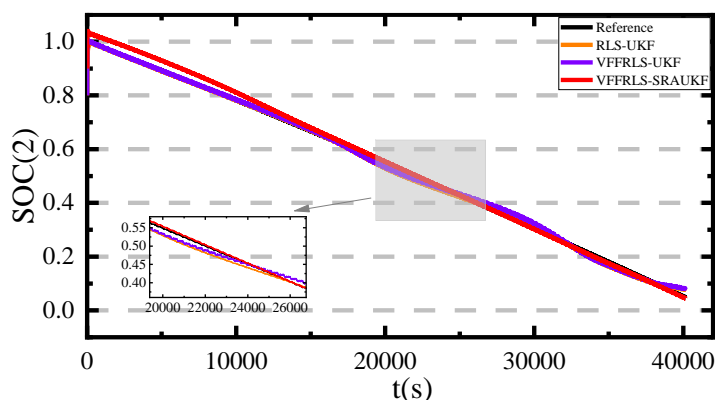
(a) SOC estimation results of BBDST condition by different algorithms
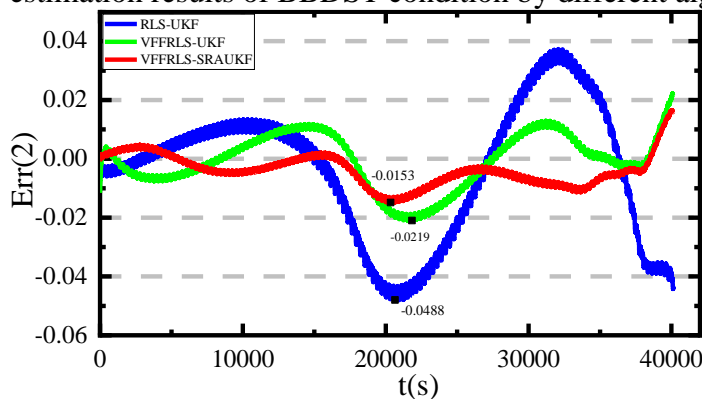
(b) SOC estimation error of BBDST condition by different algorithms

Figure 6. SOC estimation results under BBDST working condition

For verifying the estimation effect of the method, an experimental analysis is performed under BBDST conditions. The power of each step is reduced to simulate the BBDST condition according to the actual situation. The verification results of RLS-UKF, VFFRLS-UKF, and VFFRLS-SRAUKF under BBDST working condition are shown in Figure 6.

As shown in Figure 6 (b), the maximum error of SOC estimation of RLS-UKF, VFFRLS-UKF, and VFFRLS-SRAUKF algorithm is 4.88%, 2.19% and 1.53%, respectively. The estimation accuracy of the VFFRLS-UKF algorithm is about 2.69%, which is higher than that of the RLS-UKF algorithm, indicating that the variable forgetting factor is introduced to eliminate Gaussian noise in the data as much as possible, enhancing the system robustness and improving the identification accuracy. The VFFRLS-SRAUKF algorithm estimates the best accuracy and stability, reflecting the generalization of the square root adaptive algorithm in SOC estimation. The large estimation error at the discharge end is caused by heavy chemical reactions within the battery. The estimation results of the three algorithms under BBDST conditions are compared by maximum error, MAE, and RMSE, as shown in Table 2. Compared with the above experiments, it is known that the VFFRLS-SRAUKF algorithm has great accuracy and function.

Table 2. SOC estimation results of different algorithms under BBDST operating conditions are compared

Estimation method	RLS-UKF	VFFRLS-UKF	VFFRLS-SRAUKF
MAX error	4.88%	2.19%	1.53%
MAE	1.64%	0.81%	0.50%
RMSE	2.16%	0.97%	0.65%

4. CONCLUSION

The precise estimation of lithium battery SOC is the key and difficult point of the BMS. In this study, considering the current change and the noise characteristics of different working conditions, the VFFRLS algorithm is recommended for parameter identification, combined with the square root adaptive UKF algorithm for the SOC estimation of lithium-ion batteries. This algorithm is validated for SOC estimation under the HPPC and BBDST working conditions, respectively. The validation results show that when the system is stable, the VFFRLS-SRAUKF algorithm can have a maximum error of 1.41% and 1.53% under the HPPC and BBDST conditions, respectively, greatly improving the accuracy of the SOC estimation. The proposed algorithm has great convergence, avoids the dependence on experimental data in practical application, reduces the computational complexity, and can provide a reference for BMS. In future studies, multi-state joint estimation of battery packs over a long time and wide temperature range should be further explored.

References

1.   W. Zhang, L. Wang, L. Wang and C. Liao, *Journal of Power Sources*, 402 (2018) 422.
2.   T. Morstyn, M. Momayyezan, B. Hredzak and V. G. Agelidis, *Ieee Transactions on Power Electronics*, 31 (2016) 7986.
3.   B. Homan, M. V. ten Kortenaar, J. L. Hurink and G. J. M. Smit, *Energy*, 171 (2019) 205.
4.   W. H. Xu, S. L. Wang, C. Jiang, C. Fernandez, C. M. Yu, Y. C. Fan and W. Cao, *International Journal of Energy Research*, 45 (2021) 14592.
5.   S. L. Wang, X. Xiong, C. Y. Zou, L. Chen, C. Jiang, Y. X. Xie and D. I. Stroe, *International Journal of Energy Research*, 45 (2021) 17609.
6.   X. Xiong, S. L. Wang, C. Fernandez, C. M. Yu, C. Y. Zou and C. Jiang, *International Journal of Energy Research*, 44 (2020) 11385.
7.   H. Ji, W. Zhang, X. H. Pan, M. Hua, Y. H. Chung, C. M. Shu and L. J. Zhang, *International Journal of Energy Research*, 44 (2020) 6502.
8.   F. C. Sun, X. S. Hu, Y. Zou and S. G. Li, *Energy*, 36 (2011) 3531.
9.   P. Shen, M. G. Ouyang, L. G. Lu, J. Q. Li and X. N. Feng, *Ieee Transactions on Vehicular Technology*, 67 (2018) 92.
10.   C. Jiang, S. L. Wang, B. Wu, C. Fernandez, X. Xiong and J. Coffie-Ken, *Energy*, 219 (2021) 652.
11.   E. Chemali, P. J. Kollmeyer, M. Preindl, R. Ahmed and A. Emadi, *Ieee Transactions on Industrial Electronics*, 65 (2018) 6730.
12.   F. F. Yang, S. H. Zhang, W. H. Li and Q. Miao, *Energy*, 201 (2020) 5236.
13.   K. L. Liu, Y. L. Shang, Q. Ouyang and W. D. Widanage, *Ieee Transactions on Industrial Electronics*, 68 (2021) 3170.
14.   R. Xiong, J. Y. Cao, Q. Q. Yu, H. W. He and F. C. Sun, *Ieee Access*, 6 (2018) 1832.
15.   H. H. Pan, Z. Q. Lu, W. L. Lin, J. Z. Li and L. Chen, *Energy*, 138 (2017) 764.
16.   J. L. Xie, J. C. Ma and K. Bai, *Journal of Power Electronics*, 18 (2018) 910.
17.   Z. Chen, M. M. Sun, X. Shu, R. X. Xiao and J. W. Shen, *Applied Sciences-Basel*, 8 (2018) 451.
18.   Y. Li, H. Guo, F. Qi, Z. P. Guo and M. Y. Li, *Ieee Access*, 8 (2020) 17535.
19.   J. P. Tian, R. Xiong, W. X. Shen and F. C. Sun, *Energy Storage Materials*, 37 (2021) 283.
20.   S. L. Wang, C. Fernandez, L. P. Shang, Z. F. Li and H. F. Yuan, *Transactions of the Institute of Measurement and Control*, 40 (2018) 1892.
21.   X. Lai, D. D. Qiao, Y. J. Zheng and L. Zhou, *Applied Sciences-Basel*, 8 (2018) 533.
22.   A. G. Kashkooli, H. Fathiannasab, Z. Y. Mao and Z. W. Chen, *Journal of the Electrochemical Society*, 166 (2019) A605.
23.   Z. W. Deng, X. S. Hu, X. K. Lin, Y. H. Che, L. Xu and W. C. Guo, *Energy*, 205 (2020) 7651.
24.   J. C. A. Anton, P. J. G. Nieto, C. B. Viejo and J. A. V. Vilan, *Ieee Transactions on Power Electronics*, 28 (2013) 5919.
25.   C. Vidal, P. Malysz, P. Kollmeyer and A. Emadi, *Ieee Access*, 8 (2020) 52796.
26.   K. L. Liu, K. Li, Q. Peng and C. Zhang, *Frontiers of Mechanical Engineering*, 14 (2019) 47.
27.   Y. J. Wang, J. Q. Tian, Z. D. Sun, L. Wang, R. L. Xu, M. C. Li and Z. H. Chen, *Renewable & Sustainable Energy Reviews*, 131 (2020) 9713.
28.   L. F. Zheng, J. G. Zhu, G. X. Wang, D. D. C. Lu and T. T. He, *Energy*, 158 (2018) 1028.
29.   C. Huang, Z. H. Wang, Z. H. Zhao, L. Wang, C. S. Lai and D. Wang, *Ieee Access*, 6 (2018) 27617.
30.   R. Xiong, Y. Z. Zhang, H. W. He, X. Zhou and M. G. Pecht, *Ieee Transactions on Industrial*

Electronics, 65 (2018) 1526.
31. X. T. Liu, C. Y. Zheng, J. Wu, J. H. Meng, D. I. Stroe and J. J. Chen, *Energies*, 13 (2020) 4586.
32. M. Li, Y. J. Zhang, Z. L. Hu, Y. Zhang and J. Zhang, *Sensors*, 21 (2021) 8732.
33. H. Wang, Y. P. Zheng and Y. Yu, *Processes*, 9 (2021) 522.
34. Q. Zhu, M. G. Xu, W. Q. Liu and M. Q. Zheng, *Energy*, 187 (2019) 731.
35. Z. L. Zhang, X. Cheng, Z. Y. Lu and D. J. Gu, *Ieee Transactions on Power Electronics*, 32 (2017) 7626.
36. F. Liu, J. Ma, W. X. Su, H. N. Chen and M. W. He, *Energies*, 13 (2020) 4580.
37. Y. L. Zheng, F. He and W. L. Wang, *Electronics*, 8 (2019) 421.
38. M. S. El Din, A. A. Hussein and M. F. Abdel-Hafez, *Ieee Transactions on Transportation Electrification*, 4 (2018) 408.
39. X. B. Peng, Y. W. Li, W. Yang and A. Garg, *Journal of Electrochemical Energy Conversion and Storage*, 18 (2021) 642.
40. X. Y. Lin, Y. L. Tang, J. Ren and Y. M. Wei, *Journal of Energy Storage*, 41 (2021) 227.
41. X. Wei, Y. M. Mo and Z. Feng, *Integrated Ferroelectrics*, 200 (2019) 59.
42. X. W. Guo, X. Z. Xu, J. H. Geng, X. Hua, Y. Gao and Z. Liu, *Applied Sciences-Basel*, 9 (2019) 341.
43. J. P. Tian, R. Xiong, W. X. Shen and J. Wang, *Chinese Journal of Mechanical Engineering*, 33 (2020) 4791.
44. X. S. Hu, S. B. Li and H. Peng, *Journal of Power Sources*, 198 (2012) 359.
45. Y. J. Zheng, W. K. Gao, M. G. Ouyang, L. G. Lu, L. Zhou and X. B. Han, *Journal of Power Sources*, 383 (2018) 50.
46. H. Pang, L. Guo, L. X. Wu and X. F. Jin, *International Journal of Energy Research*, 44 (2020) 7254.
47. N. Koirala, F. X. He, W. X. Shen and Ieee, presented at the 10th IEEE Conference on Industrial Electronics and Applications, Auckland, NEW ZEALAND, 51 (2015) 1142.
48. Y. F. Geng, H. Pang and X. F. Liu, *Journal of Power Electronics* 9 (2020) 138.
49. P. Lin, P. Jin, A. X. Zou and Z. P. Wang, *International Journal of Energy Research*, 45 (2021) 9351.
50. Y. H. Chiang, W. Y. Sean and J. C. Ke, *Journal of Power Sources*, 196 (2011) 3921.
51. H. W. He, R. Xiong, H. Q. Guo and S. C. Li, *Energy Conversion and Management*, 64 (2012) 113.
52. K. Wang, C. L. Liu, J. R. Sun, K. Zhao, L. C. Wang, J. Y. Song, C. X. Duan and L. W. Li, *Complexity*, 2021 (2021) 9712.
53. C. Fang, Z. Jin, J. Wu and C. Liu, *Frontiers in Energy Research*, 9 (2021) 2431.
54. L. He, M. K. Hu, Y. J. Wei, B. J. Liu and Q. Shi, *Science China-Technological Sciences*, 63 (2020) 410.